Structure of the S100A6 Complex with a Fragment from the C-Terminal Domain of Siah-1 Interacting Protein: A Novel Mode for S100 Protein Target Recognition[†,‡]

Young-Tae Lee,[§,||] Yoana N. Dimitrova,[§,||] Gabriela Schneider,[⊥] Whitney B. Ridenour,[§] Shibani Bhattacharya,[§,||,@] Sarah E. Soss,[§,||] Richard M. Caprioli,[§,#] Anna Filipek,[⊥] and Walter J. Chazin*[,§,||,#]

Departments of Biochemistry and Chemistry and Center for Structural Biology, Vanderbilt University, Nashville, Tennessee 37232-8725, Department of Molecular and Cellular Neurobiology, Nencki Institute of Experimental Biology, 02-093 Warsaw, Poland, and New York Structural Biology Center, New York, New York 10027-7556

Received June 30, 2008; Revised Manuscript Received August 1, 2008

ABSTRACT: S100A6 is a member of the S100 subfamily of EF-hand Ca^{2+} binding proteins that has been shown to interact with calcyclin binding protein/Siah-1 interacting protein (CacyBP/SIP or SIP), a subunit of an SCF-like E3 ubiquitin ligase complex (SCF-TBL1) formed under genotoxic stress. SIP serves as a scaffold in this complex, linking the E2-recruiting module Siah-1 to the substrate-recruiting module Skp1-TBL1. A cell-based functional assay suggests that S100A6 modulates the activity of SCF-TBL1. The results from the cell-based experiments could be enhanced if it were possible to selectively inhibit S100A6−SIP interactions without perturbing any other functions of the two proteins. To this end, the structure of the S100A6−SIP complex was determined in solution by NMR and the strength of the interaction was characterized by isothermal titration calorimetry. In an initial step, the minimal S100A6 binding region in SIP was mapped to a 31-residue fragment (Ser189−Arg219) in the C-terminal domain. The structure of the S100A6−SIP(189−219) complex revealed that SIP(189−219) forms two helices, the first of which (Met193−Tyr200) interacts with S100A6 in a canonical binding mode. The second helix (Met207−Val216) lies over the S100A6 dimer interface, a mode of binding to S100A6 that has not previously been observed for any target bound to an S100 protein. A series of structure-based SIP mutations showed reduced S100A6 binding affinity, setting the stage for direct functional analysis of S100A6−SIP interactions.

S100 proteins make up a distinct class of the EF-hand family of Ca^{2+} regulatory proteins. Unlike the ubiquitous EF-hand Ca^{2+} sensor calmodulin, S100 proteins are distributed in a tissue- and cell type-specific manner. S100 proteins have been proposed to serve as specialized Ca^{2+} signaling factors that act in parallel with the more distributed cellular Ca^{2+} sensors such as calmodulin (*1*). Like calmodulin, S100 proteins are comprised of helix−loop−helix EF-hand domains, but they are distinguished by the formation of highly integrated dimers and less drastic conformational changes upon binding a Ca^{2+} ion relative to calmodulin and other typical Ca^{2+} sensors (*2*). These fundamental differences in structural architecture and Ca^{2+}-induced conformational changes contribute to the target specificity of S100 proteins (*3, 4*). Although considerable biochemical and biological studies have been performed over many years, a general understanding of the function of S100 proteins in the global cellular context has remained frustratingly difficult to develop (*5*).

S100A6 is one of the most well-studied S100 proteins. Originally identified as a gene whose mRNA levels change with the cell cycle and termed calcyclin (*6*), S100A6 has been shown to interact with a variety of different cytosolic proteins (reviewed in refs *4* and *7*). One such target was originally identified as calcyclin binding protein (CacyBP)[1] (*8*) and was subsequently shown to correspond to Siah-1

[†] This work was supported by operating grants from the National Institutes of Health (NIH) to W.J.C. (RO1 GM62112 and RO1 GM75156) and R.M.C. (RO1 GM58008) and from the Ministry of Science and Higher Education of Poland to A.F. (2 P04A 01030). S.E.S. is supported by an NIH training grant (T32 CA09582), and G.S. is a recipient of a scholarship from the President of the Polish Academy of Sciences. Support for facilities was provided by grants to the Vanderbilt-Ingram Cancer Center (P30 CA68485) and the Vanderbilt Center in Molecular Toxicology (P50 ES00267).

[‡] The chemical shift assignments, restraints, and atomic coordinates have been deposited in the BioMagResBank (15418) and the Protein Data Bank (2JTT).

* To whom correspondence should be addressed: Center for Structural Biology, Vanderbilt University, 465 21st Ave., Suite 5140, Nashville, TN 37232-8725. Telephone: (615) 936-2210. Fax: (615) 936-2211. E-mail: walter.chazin@vanderbilt.edu.

[§] Department of Biochemistry, Vanderbilt University.

[||] Center for Structural Biology, Vanderbilt University.

[⊥] Nencki Institute of Experimental Biology.

[@] New York Structural Biology Center.

[#] Department of Chemistry, Vanderbilt University.

[1] Abbreviations: BS^3, bis(sulfosuccinimidyl) suberate; CacyBP or SIP, Siah interacting protein; CS, CHORD and Sgt1; E2, ubiquitin conjugating enzyme; E3, ubiquitin ligase; EDTA, ethylenediaminetetraacetic acid; ESI-oaTOF, electrospray ionization orthogonal accelerating time-of-flight; GAPDH, glyceraldehyde 3-phosphate dehydrogenase; HSQC, heteronuclear single-quantum coherence; ITC, isothermal titration calorimetry; MG-132, *N*-carbobenzoxyl-Leu-Leu-leucinal; NMR, nuclear magnetic resonance; NOESY, nuclear Overhauser enhancement spectroscopy; rMD, restrained molecular dynamics; rmsd, root-mean-square deviation; SCF, Skp1-Cullin-F-box; SCF-TBL1, Skp1-Cullin-F-box-like TBL1(F-box) ubiquitin ligase; SDS−PAGE, sodium dodecyl sulfate−polyacrylamide gel electrophoresis; siRNA, small interfering RNA; TBL-1, transducin β-like protein 1; TFE, 2,2,2-trifluoroethanol; TOCSY, total correlation spectroscopy; TRTK, thymus receptor tyrosine kinase.

10.1021/bi801233z CCC: $40.75
Published on Web 09/20/2008

interacting protein (SIP), a component of the SCF-TBL1 E3 ubiquitin ligase that polyubiquitinates β-catenin in a unique phosphorylation-independent manner (*9*). CacyBP/SIP (hereafter termed SIP) is a modular protein comprised of three independent domains connected by flexible linkers: a helical hairpin N-terminal domain (M1−N78), an Hsp90 cochaperone p23-like CS (CHORD and Sgt1) domain (Y79−K177), and an intrinsically disordered SGS (Sgt1-specific) domain (E178−F229) (*8, 10, 11*). SGS domains are found in a range of proteins associated with protein ubiquitination (*9, 12, 13*), and binding to S100 proteins has been demonstrated for Sgt1 (*14*) and SIP (*15*). The S100A6 binding to the SGS domain of SIP was shown to be strictly dependent on Ca^{2+} (*8*).

Thus far, the only known function of SIP is to serve as a scaffold in the multiprotein SCF-TBL1 E3 ligase (*9*). The complex is formed under conditions of genotoxic stress, when increased levels of p53 induce the production of Siah-1, the limiting component of SCF-TBL1. Siah-1 serves as an E2-recruiting factor and also binds SIP, which serves as a scaffold linking this assembly to the substrate binding portion of the complex. The substrate β-catenin is recruited by the F-box protein TBL1, which is bound to the Skp1 adaptor protein. Interactions between SIP and Skp1 provide the final link between the E2 and substrate-recruiting modules. The complex is termed SCF-like because it has several features distinguishing it from classic SCF (Skp-cullin-F-box) complexes. Chief among these is the fact that the scaffold protein SIP is considerably smaller than all known cullins, which implies a unique architecture for SCF-TBL1.

S100 proteins have been implicated in the cytoskeleton-driven changes in cell shape, inhibition of enzyme activity, and modulation of signaling proteins (*1*). The association of S100 with protein ubiquitination represents a new direction for S100 protein function that clearly warrants further investigation. Here we report an initial cell-based experiment, suggesting that S100A6 modulates the activity of SCF-TBL1. To advance functional analysis, detailed mapping of the S100A6−SIP interaction was undertaken and the three-dimensional structure of the complex was determined in solution by NMR. Structure-based mutations that selectively inactivate the S100A6−SIP interaction were designed and tested using isothermal titration calorimetry to determine the effect on binding affinity. The implications of these results are discussed in the context of the potential role of S100A6 in the regulation of the activity of the SCF-TBL1 E3 ubiquitin ligase.

METHODS

siRNA, Transfection, and Western Blotting. Human HEp-2 cells stably transfected with the plasmid expressing siRNA against S100A6 (S100A6−) and control cells stably transfected with plasmid expressing nonspecific siRNA (S100A6+) (*45*) were grown in DMEM containing 10% fetal bovine serum, 25 mM sodium bicarbonate, penicillin (100 units/mL), streptomycin (10 μg/mL), and 200 μg/mL hygromycin B.

HEp-2 (S100A6+/−) cells (70−80% confluent) in 6 and 2.5 cm dishes were transfected with 4 or 2 μg of the expression plasmids: pFLAG-CMV-4 (Sigma) or pSiah-1-FLAG using lipofectamine 2000 (Invitrogen). After 16 h, the cells on 2.5 cm dishes were treated with 10 μM MG-132 for 8 h. Then cells were washed twice with phosphate-buffered saline. The extracts were prepared as described by Matsuzawa and Reed (*9*). Briefly, cells from 6 cm dishes were harvested and homogenized mechanically 30 times using a syringe with a needle (25 gauge, 0.5 mm × 15 mm) in buffer containing 10 mM Tris (pH 7.5), 10 mM KCl, 0.1 mM EDTA, and protease inhibitors (protease inhibitor cocktail, Complete Mini EDTA-free, Roche). Cells from 2.5 cm dishes were harvested and homogenized in the same buffer supplemented with 20 μM MG-132. The extracts were centrifuged for 30 min at 16000*g* and 4 °C; 40 μg of the protein in supernatant was loaded on each lane of SDS gel except for S100A6 assays (150 μg).

Separated proteins were transferred electrophoretically onto nitrocellulose and identified using appropriate primary antibodies: goat anti-Siah-1 antibody (1:250) (Abcam), mouse anti-β-catenin antibody (1:500) (BD Transduction Laboratories), mouse anti-S100A6 antibody (1:500) (Sigma), and mouse anti-GAPDH antibody (1:10,000) (Chemicon International). The intensities of the protein bands were quantified using the Ingenius densitometer and Gene Tools (Syngene) with GAPDH as a reference protein.

Expression Plasmids. To produce SIP and SIP fragments, mouse SIP DNA was amplified with overhanging 5′ BamHI and 3′ XhoI restriction sites for subcloning into pBG vectors created by L. Mizoue (Center for Structural Biology, Vanderbilt University). SIP(1−229), SIP(1−178), SIP(178−229), and SIP mutants were subcloned into the pBG100 vector, which produces an N-terminal His-tag fusion protein. SIP(189−219), SIP(189−203), and SIP(203−219) were subcloned into the pBG102 vector, which produces on N-terminal His- and SUMO-tag fusion protein. Intact rabbit S100A6 was produced from the pET1120 vector as described previously (*16*).

Protein Purification. The SIP proteins and S100A6 were overexpressed in BL21(DE3) and BL21(DE3)pLysS *Escherichia coli* strains, respectively. S100A6 was purified by hydrophobic interaction chromatography using a phenyl sepharose column (Amersham Biosciences) as described previously (*16*). SIP N-terminal His-tag fusion proteins were purified with a His-Select column (Sigma-Aldrich), and the His-tag was cleaved with H3C precision protease. A second purification with the same column removed the cleaved His-tag and the H3C protease, which contains a noncleavable His-tag. The proteins were dialyzed against appropriate buffers and concentrated for further studies. Protein concentrations were determined using a calculated extinction coefficient for each protein. Protein samples for NMR experiments were expressed in minimal medium with NH_4Cl and glucose as the sole nitrogen and carbon sources, respectively. $^{15}NH_4Cl$ and [$^{13}C_6$]glucose (Cambridge Isotope Laboratories) were used as needed to prepare the requisite isotopically enriched proteins.

Isothermal Titration Calorimetry. Heats of binding were measured with a Microcal VP-ITC instrument at 25 °C. The buffer contained 20 mM Tris (pH 7.0), 100 mM NaCl, 10 mM Ca^{2+}, and 1 mM DTT. Twenty-five aliquots of 10 μL of 400−600 μM SIP or its fragments were injected into 40 μM S100A6. Heats of dilution were measured in a separate experiment in which SIP was injected into the buffer. This value or the average of data points from a stable saturated baseline at the end of the titration was subtracted from all

the data points. Software provided by the vendor was used to calculate the binding affinity.

Chemical Cross-Linking. S100A6 and SIP(189−219) (0.1 mM each) were chemically cross-linked by adding equivalent molar amounts of bis(sulfosuccinimidyl)suberate (BS^3) (Pierce) in a buffer containing 50 mM Hepes (pH 7.5) and 10 mM Ca^{2+} for 1−30 min. Isolated S100A6 and SIP(189−219) were also cross-linked using the same protocol for 30 min. All cross-linking reactions were carried out at room temperature and stopped by adding SDS−PAGE loading buffer. The cross-linked products were analyzed by SDS−PAGE.

Electrospray Mass Spectrometry. Experiments were conducted with an ESI-oaTOF (electrospray ionization orthogonal accelerating time-of-flight) mass spectrometer (micrOTOF, Bruker Daltonics, Inc., Billerica, MA), which has been modified for enhanced collisional cooling in the source for the analysis of noncovalent protein complexes. The modification involved adding a valve in the turbo pump line restricting vacuum. The standard instrument parameters were used with the exception of the capillary voltage and fore pressure, which were set to 3.5 kV and 4.78 mbar, respectively. The ESI flow rate was 180 μL/h. Spectra were acquired in positive polarity mode, externally calibrated, and processed using DataAnalysis (Bruker Daltonics, Inc.) by smoothing and baseline subtraction.

NMR Spectroscopy. NMR experiments were conducted using Bruker Avance 500, 600, and 800 MHz spectrometers with Z-axis gradient TXI cryoprobes. The NMR chemical shift perturbation assays employed ^{15}N-labeled S100A6 and unlabeled SIP(189−219). The initial NMR samples contained 0.1 mM ^{15}N-labeled S100A6, 50 mM Tris (pH 6.5) (95% H_2O, 5% D_2O), and 10 mM Ca^{2+}. Concentrated SIP peptide (5−10 mM) in the same buffer was added to the ^{15}N-labeled S100A6 until the molar ratio reached 1:5 (S100A6:SIP peptide). The chemical shift perturbation was monitored by ^{15}N−^{1}H HSQC at 30 °C. The normalized chemical shift change was calculated using the equation $\Delta\sigma = \sqrt{[(\Delta H)^2 + (\Delta N/5)^2]}$, where ΔH and ΔN are chemical shift changes in proton and nitrogen dimensions, respectively.

To obtain backbone resonance assignments of SIP(189−219) bound to S100A6, 1 mM ^{15}N- and ^{13}C-labeled SIP(189−219) and 1 mM unlabeled S100A6 were prepared in 50 mM d_{11}-Tris (pH 6.5) (93% H_2O, 5% D_2O, 2% d_2-TFE) and 10 mM Ca^{2+}. ^{15}N−^{1}H HSQC, HNCA, HNCACB, CBCA(CO)NH, and HNCO experiments (*17*) were conducted at 45 °C. To obtain the side chain resonance assignments of SIP(189−219) bound to S100A6, 1 mM ^{13}C-labeled SIP(189−219) and 1 mM unlabeled S100A6 were prepared in 50 mM d_{11}-Tris (pH 6.5) (98% D_2O, 2% d_2-TFE) and 10 mM Ca^{2+}. ^{13}C−^{1}H HSQC and 3D HCCH-TOCSY experiments were carried out at 45 °C. Assigned resonances were deposited at the Biological Magnetic Resonance Data Bank as entry 15418.

To assign intramolecular NOEs in SIP(189−219), a three dimensional (3D) ^{15}N-separated NOESY-HSQC spectrum was acquired for an NMR sample containing 1 mM ^{15}N-labeled SIP(189−219) and 1 mM unlabeled S100A6, and a 3D ^{13}C-separated NOESY-HSQC spectrum was acquired for the NMR sample with 1 mM ^{13}C-labeled SIP(189−219) and 1 mM unlabeled S100A6. To distinguish intermolecular NOEs from intra-SIP(189−219) NOEs, ^{13}C-separated NOESY-HSQC spectra were acquired both with and without heteronuclear decoupling during the indirect t_1 acquisition period. Peaks that were not split in the absence of decoupling could be assigned to intermolecular NOEs. Additional intermolecular NOEs were obtained via 3D ^{13}C-separated, ^{15}N-separated NOESY-HSQC (*18*) using a sample containing 2.3 mM ^{15}N-labeled S100A6 and 2.3 mM ^{13}C-labeled SIP(189−219). All NMR data were processed using NMRPipe (*19*) and analyzed with Sparky (*20*).

Structure Calculations. Intramolecular SIP(189−219) NOEs were converted to upper limit distances using the CALIBA module in CYANA (*21*). The reference volume determined by CALIBA was increased 5 times before conversion in order to loosen the distance restraints. All upper limit distances for intermolecular NOEs were set to 6 Å. Backbone torsion angle restraints for SIP(189−219) were estimated by using TALOS (*22*). Torsion angle restraints of −110° and −30° for ϕ and −80° and 0° for ψ were added for SIP residues 213−217 on the basis of NOE connectivity. Distance and torsion angle constraints for S100A6 were obtained from previous work on the S100A6 structure (PDB entry 2JWD).

To perform CYANA calculations, a single polypeptide chain was constructed for the two S100A6 subunits and the two SIP(189−219) molecules. Five hundred structures were generated using CYANA calculations, and the 50 structures with the lowest target function were selected for further restrained molecular dynamics (rMD) using AMBER 9 (*23*) with implicit treatment of the water solvent. After energy minimization for 1 ps to regularize the structure in the AMBER force field, the temperature of the system was rapidly increased to 1200 K over 5 ps and then slowly decreased to 0 K over 15 ps. NMR restraints were gradually turned on during first 3 ps and kept for the rest of the simulation. Force constants for distance and torsion angle constraints were set to 32 and 50 kcal/mol, respectively. To select the final representative ensemble of conformers, the structures were placed in order of increasing restraint violation energy and the top 20 were selected. These structures were inspected for any local regions of high restraint violation. As a result of this analysis, nine were rejected and the next best conformers were added to the ensemble. The quality of the final ensemble was assessed using Procheck-NMR. The final ensemble of 20 conformers was deposited in the Protein Data Bank as entry 2JTT.

RESULTS

Evidence for the Functional Relevance of the S100A6−SIP Interaction. Knowing that SIP is a component of the SCF-TBL1 E3 ubiquitin ligase and that it binds S100A6, we set out to determine if S100A6 modulates the activity of the E3 ligase to establish the functional relevance of the S100A6−SIP interaction. The strategy used to address this issue involved investigating how changes in the level of S100A6 in cells alter the activity of SIP and SCF-TBL1. The read-out of this experiment is the corresponding level of the substrate β-catenin, which would be reduced if the E3 ubiquitin ligase activity is stimulated or increased if the activity of the E3 enzyme is inhibited. The experiments were performed in the HEp-2 cell line, which has moderate levels of S100A6. The siRNA approach was used to reduce the level of S100A6 in these cells.

As noted in the introductory section, formation of SCF-TBL1 requires the expression of Siah-1, which is normally

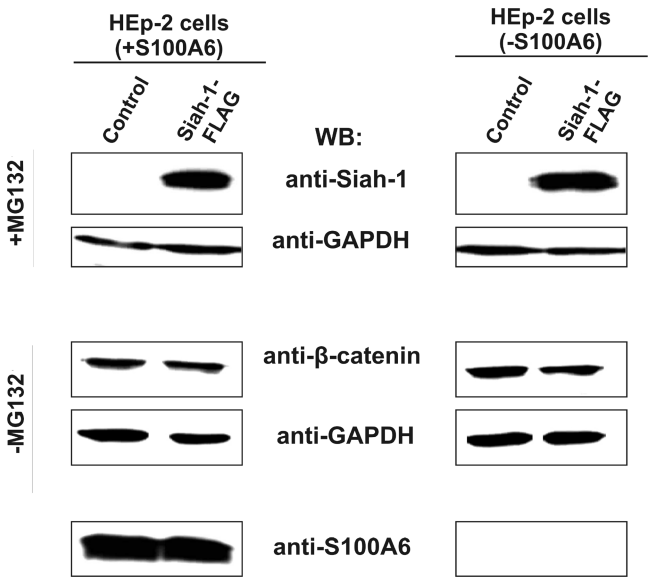

FIGURE 1: S100A6 inhibits downregulation of β-catenin by SCF-TBL1. HEp-2 cells with siRNA of S100A6 (S100A6−) and of nonspecific siRNA (S100A6+) were transfected with empty vector or pSiah-1-FLAG. Since Siah-1 is highly autoubiquitinated, a proteasome inhibitor, MG-132, was added for detection of overexpressed Siah-1.

present at very low levels in cells. Transient transfection of Siah-1 should increase the level of Siah-1 and consequently increase the amount of SCF-TBL1, which in turn should reduce the levels of β-catenin. Figure 1 shows the results of overexpressing Siah-1 by transient transfection in the HEp-2 cells. Since Siah-1 is known to be rapidly degraded in cells (*24*), a proteasome inhibitor, MG-132, was used to test if Siah-1 was overexpressed (Figure 1). Transfection of Siah-1 alone in cells with normal levels of S100A6 (S100A6+) resulted in an increase of 21% (±14%) in the levels of β-catenin (densitometric analysis from two independent experiments). In contrast, in HEp-2 cells with reduced levels of S100A6 (S100A6−), the level of β-catenin was reduced 21% (±6%). Note that these data obtained for S100A6-HEp-2 cells are consistent with results published by Matsuzawa and Reed (*9*), who reported reduced levels of β-catenin upon transfection of Siah-1 in HEK293 cells, which we confirmed have no detectable levels of S100A6. In HEp-2 cells, the activity of SCF-TBL1 increased only when S100A6 levels were suppressed. The higher levels of β-catenin in S100A6+ HEp-2 cells upon overexpression of Siah-1 versus that in S100A6− HEp-2 cells are therefore attributed to suppression of the activity of SCF-TBL1 by the presence of S100A6.

The results obtained in these experiments suggest that S100A6 does exert a measurable inhibitory effect on SCF-TBL1. However, the observed effects are modest and a considerable amount of additional cell-based evidence is required to prove the functional relevance of the S100A6−SIP interaction. The intrinsic complexity of the cell and the indirect nature of the experimental read-outs pose significant challenges in these experiments. One approach that can greatly enhance the information content of these experiments is to develop a means of selectively and specifically inhibiting the S100A6−SIP interaction without compromising other activities of the two proteins. This type of targeted mutagenesis approach would be superior to the standard approaches used such as complete knockdown of a given protein via RNAi. The advanced state of structural and biochemical knowledge of S100 proteins provides the necessary background for using such a targeted approach. Thus, a structure-based approach was pursued to enable the design of mutants that can selectively inhibit S100A6−SIP interactions without perturbing any other functions of these two proteins.

Mapping of the S100A6 Binding Site of SIP. The S100A6 binding region was previously mapped to the SGS domain of SIP (E178−F229) (*8*). The large size of the binding domain (55 residues) was intriguing as only ∼15 residues were sufficient for interaction with S100 proteins in all previously characterized complexes. In an effort to identify if S100A6 binding maps to a smaller region, binding of S100A6 to SIP and SIP fragments was tested using isothermal calorimetry (ITC).

The first ITC titration was carried out with full-length SIP, and a dissociation constant (K_d) of 5 ± 3 μM was obtained, consistent with the previous determination by fluorescence spectroscopy (∼1 μM) (*8*). ITC analysis provides not only binding affinities but also stoichiometries of binding and detailed thermodynamic parameters (Supporting Information, Table S1). Surprisingly, the binding stoichiometry determined from the ITC data was one SIP molecule per S100A6 dimer (0.5:1) as opposed to the expected stoichiometry of two molecules per dimer (1:1). This observation was not restricted to the full-length protein as similar values were obtained for all SIP fragments (Table S1). The origin of the unusual stoichiometry values derived from these data remains unknown and prompted the application of several additional approaches to confirm the expected 1:1 stoichiometry (vide infra). Because of the uncertainty in the stoichiometry values derived from the ITC data, the dissociation constants are used here only to make comparisons between different SIP fragments. Fortunately, since all of the experiments exhibit the same systematic error, the ITC analysis remains useful for comparative analyses even though there is uncertainty about the absolute values of the binding constants.

Comparison of K_d values obtained for full-length SIP and the isolated SGS domain fragment revealed they have very similar S100A6 binding affinities (Figure 2), confirming that the SIP binding region was contained strictly within the SGS domain. Sequence analysis of the SGS domain was then carried out to guide the search for a minimal binding region. Peptide fragments of S100 targets generally adapt a helical conformation once they are bound to S100 proteins (*25*−*28*), and indeed, secondary structure prediction identified two specific regions with significant helical propensity in the SGS domain: G191−E201 and D205−V216. A construct encompassing these two putative helices, SIP(189−219), was generated.

As shown in Figure 2, SIP(189−219) has an S100A6 binding affinity (5 μM) similar to that of full-length SIP and SIP-SGS. Since each putative helix in SIP(189−219) is as long as other S100-binding peptides, we asked if only one helix is sufficient for S100A6 binding. The relative binding affinity of the two helices was therefore tested using SIP fragments for each helix: SIP(189−203) and SIP(203−219). SIP(189−203) alone was able to bind S100A6 with an only 4-fold reduced binding affinity (20 μM), whereas titration with SIP(203−219) did not produce any observable heat of binding in the ITC experiments (Figure 2). These results

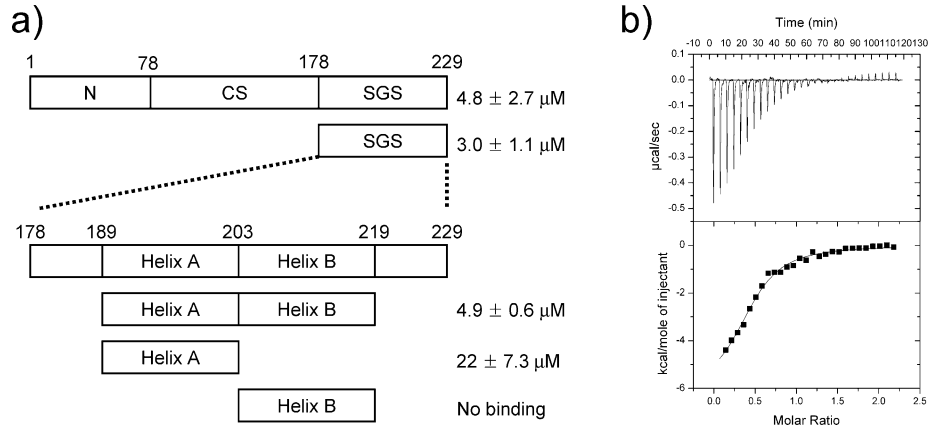

FIGURE 2: Mapping of the S100A6 binding region in SIP. (a) Binding affinity measured using isothermal titration calorimetry (ITC) for full-length SIP, SIP-SGS, SIP(189–219), SIP H-A, and H-B. (b) ITC of SIP(189−219) with S100A6. SIP(189−219) (400 μM) was titrated into 40 μM S100A6.

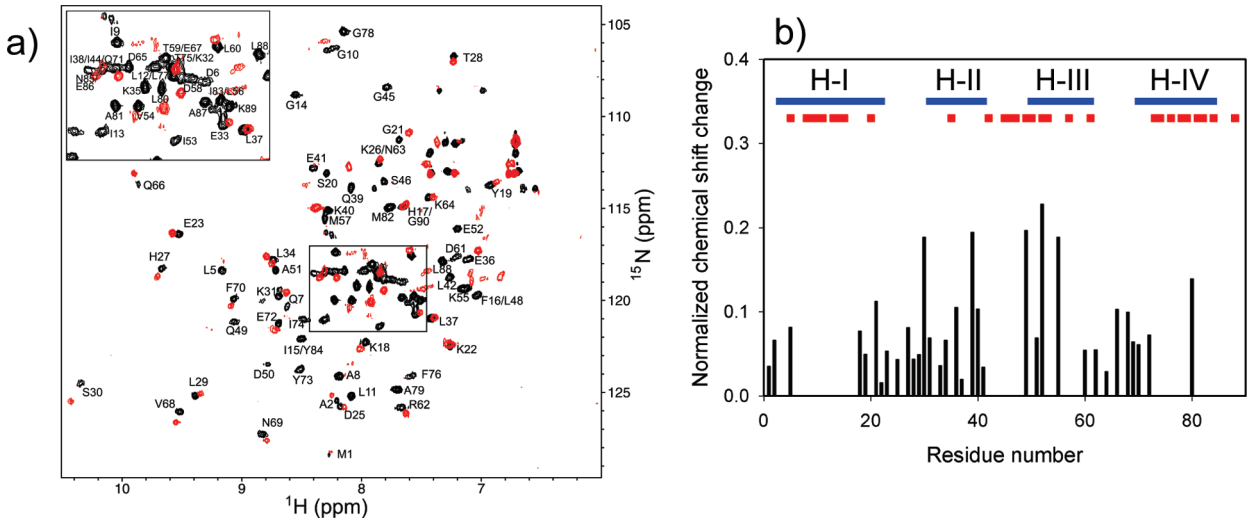

FIGURE 3: NMR chemical shift perturbation assay of the effect of SIP(189−219) binding to S100A6. (a) ^{15}N−^{1}H HSQC spectra of S100A6 acquired in the absence (black) and presence (red) of SIP(189−219). The data were collected at 30 °C on a sample containing 0.1 mM ^{15}N-labeled S100A6 and 0.5 mM SIP(189−219) in 50 mM Tris (pH 6.5) and 10 mM Ca^{2+} in a 95% H_2O/5% D_2O mixture. (b) Changes in chemical shifts in panel a plotted vs protein sequence. Blue lines are drawn for the four helices of S100A6. Red squares indicate S100A6 peaks that disappear upon addition of SIP(189−219).

show that first putative helix is required for binding to S100A6, and the second putative helix further enhances binding.

Involvement of two helices of SIP in S100A6 binding suggests that SIP binds to a larger region of the S100 protein surface than previously observed. The available structures of S100−target complexes all have a single 10−15 residue helix from the target binding at a site created by the linker between two EF-hands and helices III and IV of the C-terminal EF-hand (*25*−*28*). Since chemical shift assignments were available for S100A6, an NMR titration assay was performed to determine if the situation was similar for the S100A6−SIP(189−219) complex. When SIP(189−219) was added to ^{15}N-labeled S100A6, a large number of peaks broadened and eventually disappeared over the course of the titration while others progressively shifted (Figure 3a). These observations indicate an intermediate−fast exchange regime for the interaction. The peaks that broadened were localized to the linker, helix I (H-I), helix III (H-III), and helix IV (H-IV) of S100A6 (Figure 3b), a region significantly larger than that reported for other S100−target complexes. For example, in the structures of S100−annexin complexes (*25, 29*), only residues from the linker, H-IV of one subunit, and H-I′ of the other subunit contribute to the target binding site. Similarly, structures of complexes of S100B with target peptides from p53 (*26, 30*), TRTK-12 (*27, 31*), and Ndr kinase (*28*) revealed the target binding surface is comprised of residues from H-III, H-IV, and the linker. The combination of perturbations of a substantial part of S100A6 and the involvement of two SIP helices indicate this complex corresponds to a new mode of S100 protein−target interaction.

Two SIP Molecules Bind One S100A6 Dimer. S100 protein dimers have two symmetrically disposed target binding sites and therefore bind two target peptides per dimer. Since SIP(189−219) is larger than all previously characterized target peptides, it is conceivable that one SIP peptide could fill both binding surfaces. However, the presence of one set of NMR signals for the S100A6 dimer in the SIP(189−219) complex (Figure 3a) implies that two SIP molecules are symmetrically bound to the S100A6 dimer. Moreover, NMR titrations of SIP peptides into solutions of S100A6 were seen to saturate when two SIP molecules were present for each SIP dimer (Supporting Information, Figure S1).

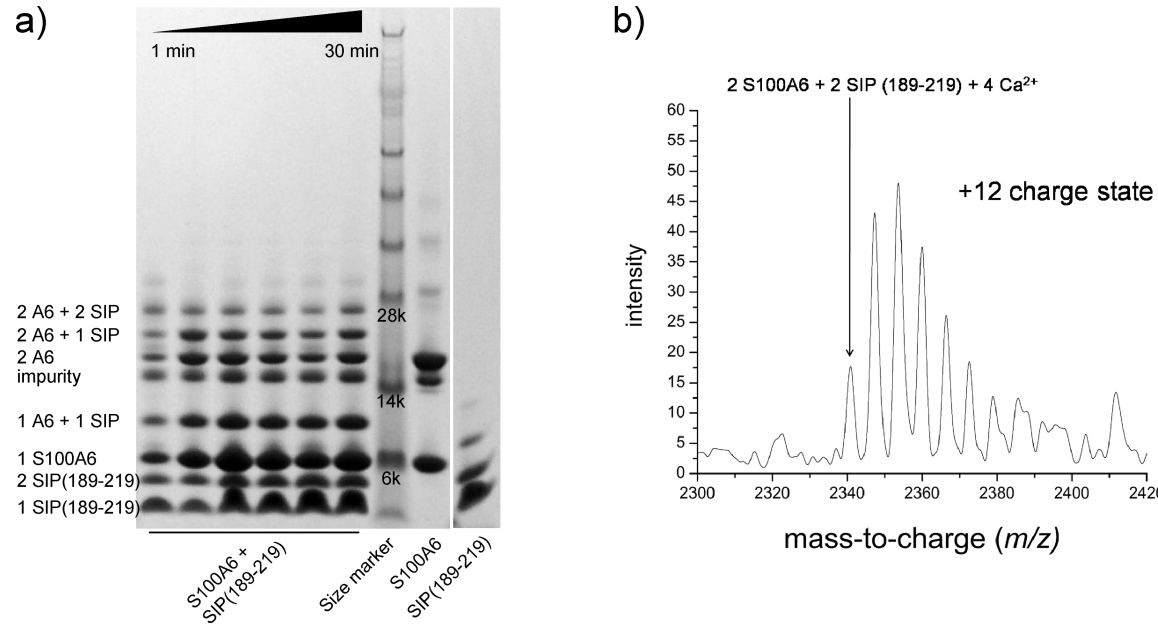

FIGURE 4: Stoichiometry of the S100A6−SIP(189−219) complex. (a) Chemical cross-linking detected by SDS−PAGE. S100A6 (0.1 mM) and SIP(189−219) (0.1 mM) were chemically cross-linked using BS^3, and aliquots were taken over a period of 1−30 min. Lanes at the right show the result of cross-linking isolated S100A6 and SIP(189−219) for 30 min. (b) Electrospray mass spectroscopy. S100A6 (0.1 mM) and SIP(189−219) (0.15 mM) were mixed in 25 mM ammonium acetate and 1 mM calcium acetate. The deconvoluted mass of the complex of two S100A6 and two SIP(189−219) molecules bound to four Ca^{2+} ions is calculated from the +8, +10, and +12 charge states to be 28081 ± 1 Da, which is consistent with the total mass of the complex.

Given the unanticipated result from the ITC analysis, two additional approaches were used to probe the stoichiometry of the complex. First, chemical cross-linking experiments were performed. The conditions were adjusted so that a limiting amount of cross-linking agent was used. Experiments were repeated over a range of concentrations of the complex to minimize intermolecular cross-links. Working with the optimized conditions, we observed a complex of two S100A6 molecules and two SIP(189−219) peptides, suggesting two SIP peptides bind per S100 dimer (Figure 4a). The presence of cross-linked dimer and trimer in control experiments on isolated SIP(189−219) leads to some ambiguity in the "2A6 + 2SIP" band, which theoretically could arise from binding of one SIP dimer to one S100A6 dimer. However, the absence of a "2A6 + 4SIP" band suggests that SIP homodimers do not bind to S100A6. Thus, the cross-linking results support but do not unambiguously prove the stoichiometry of the complex is 2:2. We therefore turned to electrospray ionization mass spectrometry (ESI-MS).

Recent developments in the use of ESI-MS have enabled the direct observation of the molecular mass of the noncovalent complexes (*32*). Experiments were performed on S100A6 complexes with both SIP(189−219) and full-length SIP. For the former, a series of ions were observed in the +12 charge state around *m*/*z* 2340−2350 corresponding to two SIP(189−219) and two S100A6 molecules, and different numbers of bound Ca^{2+} ions (Figure 4b). The smallest number of Ca^{2+} ions bound to this complex is four, corresponding to the filling of all four EF-hand domains in the S100A6 dimer. The additional Ca^{2+} ions bound to the complex are attributed to ions bound nonspecifically that are captured upon ionization of the complex. Corresponding data for the full-length SIP were similar, other than the higher molecular mass of intact SIP. Thus, the ESI-MS analysis supports the results from the NMR and cross-linking experiments, and we conclude that two SIP molecules are bound per S100A6 dimer.

Determination of the Structure of the S100A6−SIP(189−219) Complex. To identify the features of the apparently unique S100A6−SIP peptide complex, the three-dimensional structure of the complex was determined in solution by NMR. The strategy used in this case involved docking the peptide to the previously determined high-resolution solution structure of Ca^{2+}-loaded S100A6 (*33*). The rationale behind this strategy was that the rather small chemical shift perturbations induced by SIP binding indicate that the structure of S100A6 was not significantly perturbed, consistent with the many examples of structures that show the conformation of S100 proteins is minimally perturbed upon binding target peptides (*25*−*28*).

Two sets of NMR experiments were conducted for structure calculation: one focused on structural restraints within SIP(189−219) and the second on structural restraints between SIP and the S100A6 dimer. Toward this end, ^{15}N-enriched samples and ^{13}C- and ^{15}N-enriched samples of SIP(189−219) and S100A6 were produced for use in multidimensional triple-resonance NMR experiments with the complex. One challenge encountered with the NMR analysis of the S100A6−SIP complex was the considerable degree of resonance exchange broadening, which resulted in the loss of some signals in the $^{15}N-^{1}H$ HSQC spectrum of S100A6 (Figure 3). Optimized conditions required a combination of elevated temperature (45 °C) and inclusion of the organic solvent trifluoroethanol (2% TFE) for maximization of the number of observed peaks. Control experiments demonstrated that the presence of TFE in solution causes only very slight perturbations of chemical shifts of S100A6 and SIP(189−219) (Supporting Information, Figure S2).

Table 1: Structural Statistics for the Complex Structure of S100A6 and SIP(189−219)

constraints[a]	
distance (intramolecular)	
S100A6[b]	1388
intraresidue ($\|i - j\| = 0$)	1005
sequential ($\|i - j\| = 1$)	101
medium-range ($\|i - j\| = 2$, 3, or 4)	159
long-range ($\|i - j\| > 4$)	123
SIP(189−219)	349
intraresidue ($\|i - j\| = 0$)	202
sequential ($\|i - j\| = 1$)	84
medium-range ($\|i - j\| = 2$, 3, or 4)	63
angle (ϕ and ψ)	
S100A6[b]	145
SIP(189−219)	46
distance (intermolecular)	
S100A6/S100A6[b]	158
S100A6/SIP(189−219)	36
constraint violations [mean ± standard deviation (SD)]	
no. of distance violations (d)	
0.1 Å < d < 0.2 Å	7 ± 2
0.2 Å < d	0
average maximum d (Å)	0.15 ± 0.02
no. of torsion angle violations (θ)	
θ < 5°	2 ± 2
5° < θ	0
average maximum θ (deg)	3 ± 1
AMBER energies, mean ± SD (kcal/mol)	
constraint energy	13.3 ± 1.3
total energy	−8239 ± 28
Ramachandran analysis (%)	
residues in most favored regions	90.0
residues in additional allowed regions	8.1
residues in generously allowed regions	1.1
residues in disallowed regions	0.8

precision, pairwise rmsd ± SD (Å)[c]	backbone	heavy atoms
S100A6	0.78 ± 0.12	1.32 ± 0.12
SIP(189−219)	1.42 ± 0.43	2.27 ± 0.35
complex	1.09 ± 0.23	1.70 ± 0.19

[a] Number of constraints per subunit. [b] Previously obtained for Ca^{2+}-loaded S100A6 (*33*). [c] Residues in the ordered structure were used for the calculation of the rmsd: 3−21, 31−41, 50−61, and 70−82 for S100A6 and 193−200 and 207−216 for SIP(189−219).

Nearly complete assignments of backbone and side chain resonances of SIP(189−219) bound to S100A6 were made using standard two-dimensional (2D) and 3D NMR experiments. An extensive effort was then made to run the standard set of 2D and 3D filter/edited NOESY experiments on the complex. However, these experiments proved to be of uniformly low sensitivity on this system. We therefore turned to simpler approaches that provided higher sensitivity, taking advantage of the fact that spectral overlap for SIP(189−219), though significant, did not preclude analysis. In all, 349 intramolecular NOEs were assigned for SIP(189−219) bound to S100A6 [∼12 per residue (Table 1)] from 3D ^{15}N-separated and 3D ^{13}C-separated NOESY spectra. Analysis of medium-range NOEs showed that the two predicted helices are indeed present in solution with the N-terminal helix spanning Met191−Tyr200 (H-A) and the C-terminal helix spanning Arg209−Glu217 (H-B). Notably, no long-range NOEs between these two helices were observed, indicating that the two helices in SIP(189−219) do not pack together when bound to S100A6.

In addition to the intramolecular NOEs, 15 unique intermolecular NOEs were initially identified by comparing 3D ^{13}C-separated NOESY-HSQC spectra acquired with or without decoupling of carbon nuclei during indirect proton evolution on a sample containing ^{13}C-labeled SIP(189−219) and unlabeled S100A6 (Supporting Information, Figure S3a). Intramolecular NOE peaks are distinguished from intermolecular NOEs in this spectrum as only intramolecular peaks are split by the ^{13}C−^{1}H coupling constant in the "coupled" spectra (Supporting Information, Figure S3b,c). All assigned intermolecular NOEs from the strategy given above originated only from H-A of SIP so additional approaches were required. The most fruitful of these was a 3D ^{13}C-separated, ^{15}N-separated NOESY-HSQC spectrum (*18*) acquired for a complex composed of ^{15}N-labeled S100A6 and ^{13}C-labeled SIP(189−219), which provided among others 21 additional unique intermolecular NOEs, including some involving H-B.

Previously determined structures and the corresponding NMR constraints for the Ca^{2+}-loaded S100A6 were used as the structural template for docking SIP(189−219) (see Methods). Because S100A6 is a homodimer with two equivalent S100A6 subunits, there is ambiguity about some of the intermolecular NOEs. The NOEs between S100A6 and H-A indicated H-A lies between H-III and H-IV of S100A6, whereas H-B aligns with H-I. Since H-I and H-I′ are in the proximity of each other in the dimer (Figure 5b), it is unclear whether H-B binds to the same subunit of the dimer as H-A, or to the opposite subunit. The ambiguity was overcome by performing separate structure calculations for each possible arrangement and comparing the results on the basis of constraint violations. The results of these calculations were unambiguous in indicating that H-B of SIP contacts the opposite S100A6 subunit compared to that to which the corresponding H-A is bound. Once this obstacle was overcome, the refinement of the S100A6−SIP(189−219) structure proceeded in a straightforward manner.

S100A6−SIP(189−219) Structure. The final ensemble of 20 conformers representing the S100A6−SIP(189−219) structure is shown in Figure 5. Structural statistics for the ensemble indicated that there are no distance violations greater than 0.2 Å and no torsion angle violations greater than 5° (Table 1). PROCHECK-NMR analysis revealed 99.2% of residues were in the allowed regions of the Ramachandran plot, indicating that the structure of SIP(189−219) and its binding site on S100A6 is reasonably well defined (Table 1). Pairwise rmsds of backbone nuclei for S100A6, the SIP peptide, and the complex were 0.78, 1.09, and 1.42 Å, respectively (Table 1). As anticipated, the S100A6 structure is not altered in any significant way, and the two helical elements in SIP(189−219) are readily apparent. The mode of binding in the S100A6−SIP(189−219) complex is distinguished among all other S100−peptide complexes by the presence and location of H-B (vide infra).

H-A sits in the hydrophobic groove formed by H-III and H-IV of S100A6, and H-B binds to the interface formed by H-IV of one subunit of S100A6 and H-I of the other subunit (Figure 5b). Interestingly, the binding site for H-A in S100A6 is a highly concave surface (Figure 5c), whereas the binding site for H-B is relatively flat. H-A also contacts a larger number of residues in S100A6 than H-B (Figure 7). The larger binding interface between S100A6 and H-A is consistent with the ITC data indicating H-A is the primary mediator of S100A6−SIP affinity.

The binding of H-A to S100A6 is mainly driven by hydrophobic contacts (Figure 7), and there are notably fewer contributions from ionic interactions than in the S100B−p53

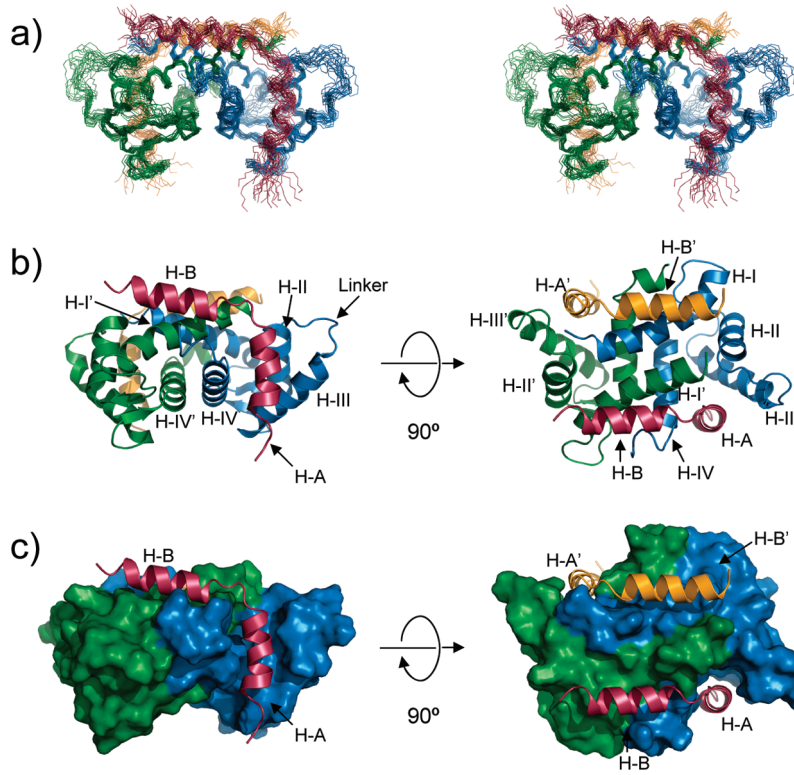

FIGURE 5: Structure of Ca^{2+}-loaded S100A6 with SIP(189−219). The two S100A6 subunits are colored blue and green (a−c). The two SIP(189−219) molecules are colored red and orange (a−c). (a) Stereoview of the backbone atoms in the final ensemble of the 20 representative conformers. (b) Ribbon diagram of the representative structure. Helices are marked by H-I−IV for one S100A6 subunit and H-I′−IV′ for the other S100A6 subunit. H-A and H-B denote the two helices of SIP(189−219). (c) Surface model of S100A6 bound to SIP(189−219) in a ribbon diagram.

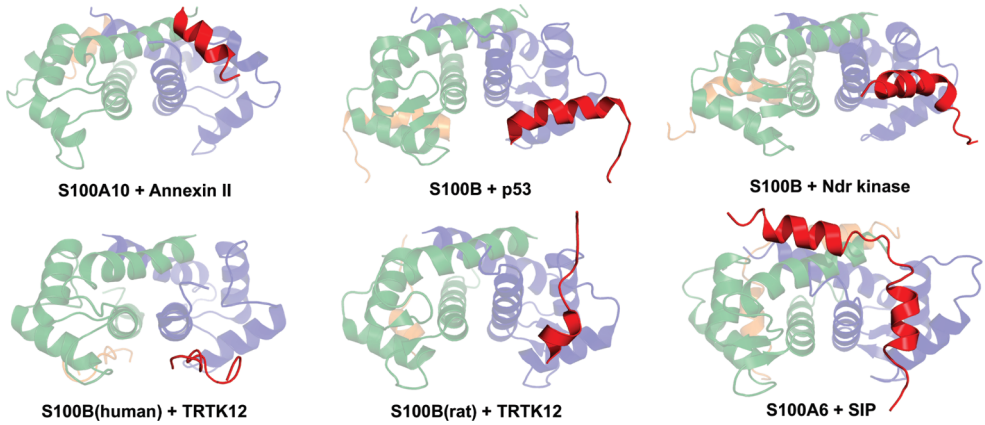

FIGURE 6: Comparison of S100 protein−target structures. Target peptides are highlighted in red. The following structures are shown: S100A10−annexin II(1−10) (PDB entry 1BT6), S100B−p53(367−388) (PDB entry 1DT7), S100B−Ndr kinase(62−87) (PDB entry 1PSB), S100B(human)−TRTK12 (PDB entry 1MQ1), S100B(rat)−TRTK12 (PDB entry 1MWN), and S100A6−SIP(189−219) (PDB entry 2JTT).

or S100B−Ndr kinase complex. Leu196 in SIP plays a very key role at the center of the hydrophobic contacts with S100A6 (Figures 7 and 8). Leu196 contacts hydrophobic S100A6 residues from H-III and H-IV, including Leu56, Phe76, Leu80, and Ile83 (Figure 8a), which form a pocket in which the side chain of Leu196 is completely buried (Figure 8b). Additional hydrophobic contacts are supplied by the adjacent residues Leu192, Met193, Val195, and Ile199, which together extend the hydrophobic surface along the length of the amphipathic helix. While Leu196 of SIP has many contacts with H-IV residues in S100A6, an adjacent residue in H-A, Ile199, interacts with S100A6 H-III and the linker through a hydrophobic surface created by Leu42, Ile44, Ile53, and Leu56 (Figure 7). SIP Leu196 and Ile199 thus appear to serve as anchoring residues to orient SIP on the S100A6 binding surface. Ile5 and Trp7 of TRTK12 and Leu383 and Phe385 of p53 have been shown to play similar roles in the S100B−TRTK12 and S100B−p53 complexes, respectively (*26, 31*). Other hydrophobic residues such as Leu192, Met193, and Val195 of SIP provide additional hydrophobic contacts with S100A6 around both H-III and H-IV (Figure 7).

The H-B binding site on S100A6 is smaller and less hydrophobic than the H-A binding site. It was anticipated that Trp215 would play a key role in the binding to S100A6 as aromatic residues of target peptides often play

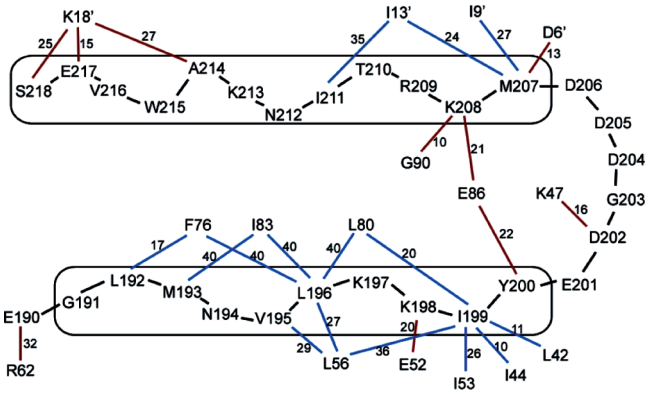

FIGURE 7: Analysis of contacts between S100A6 and SIP(189−219). Residues from the SIP peptide are linked by black lines with the two helices in rectangles. Blue lines represent hydrophobic contacts with a cutoff of 4.5 Å. Red lines represent electrostatic interactions such as hydrogen bonds or salt bridges. S100A6 residues marked by a prime represent the other subunit of S100A6. Each contact is labeled with the number of occurrences in the ensemble of 20 conformers.

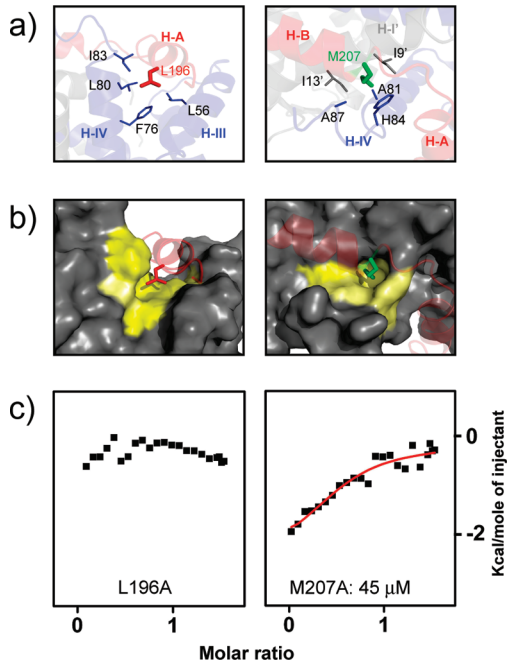

FIGURE 8: SIP Leu196 is a key residue for S100A6 binding. The binding interfaces around SIP Leu196 and Met207 are shown in (a) a ribbon diagram and (b) a surface representation. Hydrophobic residues in panel b are colored yellow and pale yellow for strong (Leu, Ile, Val, and Phe) and weak (His and Ala) hydrophobic residues, respectively. (c) ITC studies of S100A6 and SIP mutants.

an important role in binding to S100 proteins (*25*−*28*, *31*). However, Trp215 does not appear to be significantly involved. His17 and Tyr19 in S100A6 are closest to Trp215 in the S100A6−SIP(189−219) structure, but their side chains are rotated away from Trp215. This feature in the structure is supported by the lack of chemical shift changes for His17 and Tyr19 in the NMR perturbation assay (Figure 3). Instead of Trp 215, Met207 appears to be the critical hydrophobic anchor for H-B binding to S100A6. It contacts Ile9 and Ile13 in H-I′ of S100A6, and the Met side chain is completely buried upon binding to S100A6. Additional S100A6 residues contributing to the formation of the binding pocket for Met207 in S100A6 include Ala81, His84, and Ala87.

Structure-Based Design of SIP Mutants. A number of structure-based mutant designs were generated with the goal of producing single-site mutants with a reduced affinity for S100A6. Analysis of contacts in the S100A6−SIP-(189−219) structure identified two key hydrophobic residues from each helix (Leu196 in H-A and Met207 in H-B) along with several additional contributing residues (Leu192, Val195, Ile199, and Tyr200 in H-A and Ile211 in H-B). Full-length SIP constructs were prepared in which each of these residues was mutated to Ala, so specific hydrophobic contacts were deleted. Binding of S100A6 to these mutants was tested using ITC. The results for the two key hydrophobic residues (Leu196 and Met207) are presented in the following, since these proved to be the most effective mutant designs.

Substitution of Leu196 with Ala proved to be the single most potent mutation. In fact, titration of S100A6 with SIP L196A did not produce detectable heat changes in ITC experiments (Figure 8c). This observation indicates that the loss of the side chain significantly perturbs the binding interface, although because no specific measurement of the binding affinity can be made, it is not possible to determine the extent to which binding is inhibited. These results suggest that L196A will be a valuable knockout reagent for functional analysis.

Substitution of Met207 for Ala resulted in a more than 10-fold reduction in the binding affinity of SIP for S100A6 (Figure 8c). Given the similarity of the binding affinity of this mutant with that determined for the construct lacking the entire H-B helix (Figure 2) and that H-A and H-B have no contacts with each other, it is likely that the M207A mutant dislodges H-B from binding to S100A6. This confirms the central role of Met207 in SIP H-B binding to S100A6 and suggests that SIP M207A will be an effective knockdown mutant for functional analysis. The ensemble of these results also demonstrates the effectiveness of the structure-based mutant designs.

DISCUSSION

A Unique Mode of Target Binding to an S100 Protein. The S100A6−SIP complex represents a new mode of S100 protein−target interaction. This is reflected in a buried surface area at the S100A6−SIP(189−219) interface (1140 ± 69 Å) that is significantly larger than that of all other S100−target complexes whose structures have been determined [e.g., S100B−Ndr kinase (750 Å), S100B−p53 (540 Å), S100B−TRTK (523 Å), and S100A10−annexin II (683 Å)]. The much larger surface area in the S100A6−SIP(189−219) complex is a byproduct of the involvement of SIP H-B. This bipartate mode of binding is somewhat reminiscent of the "full length binding target model", which is based on a comparative structural analysis of complexes of p53 and annexin peptides (*34*). In particular, these authors noted that in the structures of these complexes, only a fraction of the hydrophobic surface in the C-terminal EF-hand is occupied. Thus, it was possible to model binding of both p53 and annexin peptides simultaneously on the structure of Ca^{2+}-loaded human S100A6 with no significant overlap. They proposed that either two target proteins or two distinct binding regions

of one target protein could bind to each of the two canonical binding sites within an S100 protein dimer. This model allows the combination of many interactions in which up to four different proteins could bind to a single S100 dimer and serve as an interface for a multiprotein complex. However, the modeling was based on peptide fragments, and it is unclear if such multimode binding events are sterically feasible with intact proteins. Moreover, to the best of our knowledge, there are no reports of two different target proteins binding to a single S100 protein at the same time. In the case of the S100A6−SIP complex, SIP H-A binds at the center of the hydrophobic groove between H-III and H-IV of S100A6, which would preclude binding of a second target molecule in the canonical site.

Until the structure of the S100A6−SIP complex was determined, all S100 protein targets were observed to bind at the hydrophobic surface created when H-III in the C-terminal EF-hand shifts upon binding of Ca^{2+}. However, the orientations of the peptide fragments in each complex vary considerably. Variability in target orientation also extends to different targets binding to a given protein, as seen, for example, in S100B complexes with p53, Ndr kinase, and TRTK 12 peptides (Figure 6). In the S100A6−SIP(189−219) structure, we find that H-A adds to this diversity: its orientation is almost perpendicular to the orientation of the p53 and Ndr kinase peptides in complex with S100B (Figure 8). While there is some similarity to the S100B complex with TRTK 12, the TRTK 12 peptide is shorter and opposite in polarity to SIP H-A. The differences in the orientation of different targets with the common binding site are a reflection of sequence variability within the S100 proteins and their targets, which we have proposed contributes significantly to the selectivity of S100 proteins for targets (*3*).

Like H-B in the S100A6−SIP complex, annexin I and II peptides bind to a surface at the S100 protein dimer interface. However, the orientation of SIP H-B is quite different from that of the annexin peptides, which are almost perpendicular to H-I, whereas H-B of SIP is almost parallel to H-I. More importantly, the annexin peptides have an extensive hydrophobic interaction with the S100 protein linker, which is absent in the S100A6−SIP complex; the binding site of SIP H-B on S100A6 does not involve any of the hydrophobic surface in the C-terminal EF-hand of S100A6. Rather, the SIP H-B binding site is created primarily by H-I in the N-terminal EF-hand. We note that the conformation of the N-terminal EF-hand is only slightly altered by Ca^{2+} binding, which suggests SIP H-B binding to S100A6 is not Ca^{2+}-dependent. Ca^{2+}-independent S100−target interactions have been observed (reviewed in ref *4*), but their binding sites on S100 proteins are largely unknown. Moreover, recent studies of S100B oligomerization in crystals revealed interactions between dimers that are not mediated by Ca^{2+} (*35*). As the plausible Ca^{2+}-independent interaction of SIP H-B is quite weak, it is not likely that H-B constitutively binds to S100A6 in the cell. However, transient interaction of H-B with S100A6 may help to localize SIP to the vicinity of S100A6 to enable rapid response to Ca^{2+} signals, along the lines of current proposals for other Ca^{2+} sensor proteins such as calmodulin. A similar mode of localization may be operative for other S100−target protein pairs.

Considerable knowledge about S100 target recognition has been generated as the result of numerous structural studies that define Ca^{2+}-dependent changes in S100 proteins and interactions with target proteins. Our studies of the S100A6−SIP complex revealed canonical binding of one helical element of SIP and a second helical element binding in a distinct site not previously observed. Thus, the diversity of ways in which S100 proteins interact with targets continues to grow, the implications of which are important for understanding the functional consequences of S100−target interactions (*5*).

Biological Implications of the SIP−S100A6 Interaction. Abnormal accumulation of β-catenin has been observed in colon cancer (*36*) and breast cancer cells (*37*). A high level of S100 proteins is implicated in certain neoplastic disorders (*38*), and a deregulation of S100A6 expression has been observed in numerous cancer cells (*39, 40*). Tissue-based experiments have shown that S100A6 is overexpressed in many breast cancer cells where β-catenin levels are high (*41*). Overexpression of SCF-TBL1 proteins, including SIP, in renal cancer cells was shown to downregulate β-catenin and suppress cellular proliferation (*42*). However, the inhibitory effect of S100A6 on the SCF-TBL1 E3 ubiquitin ligase complex could attenuate this phenomenon. Thus, deregulation of S100A6 might contribute to cancer progression by blocking β-catenin degradation through the SCF-TBL1 E3 ubiquitin ligase complex.

How can S100A6 binding to the flexible and disordered C-terminal domain of SIP affect the activity of the E3 ligase? One possibility is the SGS domain may be structurally integrated into the SCF−TBL1 complex. If so, the interaction of S100A6 with SIP could perturb the architecture of the E3 ubiquitin ligase. Recent studies have shown in vivo that the interaction of a protein highly homologous to SIP, Sgt1, with Hsp90 or Nod requires the SGS domain (*43, 44*). Moreover, a SGS domain mutant of SIP, E217K, was shown to disrupt the function of the E3 ubiquitin ligase (*9*), indicating the SGS domain is indeed important for the function of SIP within the E3 ubiquitin ligase. Thus, it is likely that S100A6 binding to SIP can perturb SCF-TBL1 and in turn the ability to ubiquitinate β-catenin.

The apparent inhibitory function of S100A6 with respect to the activity of SCF-TBL1 observed in HEp-2 cells (Figure 1), combined with the known interaction of S100A6 and SIP (*8*), suggests the need for further investigations of the functional relevance of this interaction. The binding mutants designed on the basis of the structure of the S100A6−SIP-(189−219) complex are expected to allow highly efficient testing of the importance of this interaction via in vivo experiments as well as in an in vitro ubiquitination assay.

ACKNOWLEDGMENT

We thank L. P. Slomnicki for preparing the pSilencer 2.1-U6 hygro plasmid encoding siRNA against S100A6, S. Matsuzawa and J. C. Reed for providing a plasmid encoding the Siah-1-FLAG protein, S. Matsuzawa and B. D. Carter for helpful discussions, and the reviewers for very valuable critiques.

SUPPORTING INFORMATION AVAILABLE

Thermodynamic parameters derived from the ITC experiments characterizing the binding of SIP to S100A6 (Table S1), chemical shift changes for select S100A6 residues as a

function of SIP(189–219):S100A6 monomer ratio supporting 1:1 stoichiometry (Figure S1), evidence showing addition of 2% TFE to the solution does not induce helical structure in free SIP(189−219) (Figure S2), and the strategy employed for assignments of intermolecular NOEs between S100A6 and SIP(189−219) (Figure S3). This material is available free of charge via the Internet at http://pubs.acs.org.

REFERENCES

1. Donato, R. (2003) Intracellular and extracellular roles of s100 proteins. *Microsc. Res. Techniq. 60*, 540–551.
2. Nelson, M. R., and Chazin, W. J. (1998) Structures of EF-hand Ca^{2+}-binding proteins: Diversity in the organization, packing and response to Ca^{2+} binding. *BioMetals 11*, 297–318.
3. Bhattacharya, S., Bunick, C. G., and Chazin, W. J. (2004) Target selectivity in EF-hand calcium binding proteins. *Biochim. Biophys. Acta 1742*, 69–79.
4. Santamaria-Kisiel, L., Rintala-Dempsey, A. C., and Shaw, G. S. (2006) Calcium-dependent and -independent interactions of the S100 protein family. *Biochem. J. 396*, 201–214.
5. Chazin, W. J. (2007) The impact of X-ray crystallography and NMR on intracellular calcium signal transduction by EF-hand proteins: Crossing the threshold from structure to biology and medicine. *Sci. STKE,*, pe27.
6. Hirschhorn, R. R., Aller, P., Yuan, Z. A., Gibson, C. W., and Baserga, R. (1984) Cell-cycle-specific cDNAs from mammalian cells temperature sensitive for growth. *Proc. Natl. Acad. Sci. U.S.A. 81*, 6004–6008.
7. Filipek, A., Michowski, W., and Kuznicki, J. (2007) Involvement of S100A6 (calcyclin) and its binding partners in intracellular signaling pathways. *Adv. Enzyme Regul.,* doi:10.1016.jadvenzreg.2007.11.001.
8. Nowotny, M., Bhattacharya, S., Filipek, A., Krezel, A. M., Chazin, W., and Kuznicki, J. (2000) Characterization of the interaction of calcyclin (S100A6) and calcyclin-binding protein. *J. Biol. Chem. 275*, 31178–31182.
9. Matsuzawa, S., and Reed, J. C. (2001) Siah-1, SIP, and Ebi collaborate in a novel pathway for β-catenin degradation linked to p53 responses. *Mol. Cell 7*, 915–926.
10. Bhattacharya, S., Lee, Y. T., Michowski, W., Jastrzebska, B., Filipek, A., Kuznicki, J., and Chazin, W. J. (2005) The modular structure of SIP facilitates its role in stabilizing multiprotein assemblies. *Biochemistry 44*, 9462–9471.
11. Santelli, E., Leone, M., Li, C. L., Fukushima, T., Preece, N. E., Olson, A. J., Ely, K. R., Reed, J. C., Pellecchia, M., Liddington, R. C., and Matsuzawa, S. (2005) Structural analysis of Siah1-Siah-interacting protein interactions and insights into the assembly of an E3 ligase multiprotein complex. *J. Biol. Chem. 280*, 34278–34287.
12. Kitagawa, K., Skowyra, D., Elledge, S. J., Harper, J. W., and Hieter, P. (1999) SGT1 encodes an essential component of the yeast kinetochore assembly pathway and a novel subunit of the SCF ubiquitin ligase complex. *Mol. Cell 4*, 21–33.
13. Azevedo, C., Sadanandom, A., Kitagawa, K., Freialdenhoven, A., Shirasu, K., and Schulze-Lefert, P. (2002) The RAR1 interactor SGT1, an essential component of R gene-triggered disease resistance. *Science 295*, 2073–2076.
14. Nowotny, M., Spiechowicz, M., Jastrzebska, B., Filipek, A., Kitagawa, K., and Kuznicki, J. (2003) Calcium-regulated interaction of Sgt1 with S100A6 (calcyclin) and other S100 proteins. *J. Biol. Chem. 278*, 26923–26928.
15. Filipek, A., Jastrzebska, B., Nowotny, M., and Kuznicki, J. (2002) CacyBP/SIP, a calcyclin and Siah-1-interacting protein, binds EF-hand proteins of the S100 family. *J. Biol. Chem. 277*, 28848–28852.
16. Sastry, M., Ketchem, R. R., Crescenzi, O., Weber, C., Lubienski, M. J., Hidaka, H., and Chazin, W. J. (1998) The three-dimensional structure of Ca^{2+}-bound calcyclin: Implications for Ca^{2+}-signal transduction by S100 proteins. *Structure 6*, 223–231.
17. Cavanagh, J., Fairbrother, W. J., Palmer, A. G., Skelton, N. J., and Rance, M. (2006) *Protein NMR Specroscopy: Principles and Practice*, Academic Press, New York.
18. Diercks, T., Coles, M., and Kessler, H. (1999) An efficient strategy for assignment of cross-peaks in 3D heteronuclear NOESY experiments. *J. Biomol. NMR 15*, 177–180.
19. Delaglio, F., Grzesiek, S., Vuister, G. W., Zhu, G., Pfeifer, J., and Bax, A. (1995) NMRPipe: A multidimensional spectral processing system based on UNIX pipes. *J. Biomol. NMR 6*, 277–293.
20. Goddard, T. D., and Kneller, D. G. (2006) *SPARKY 3*, University of California, San Francisco.
21. Guntert, P., Mumenthaler, C., and Wuthrich, K. (1997) Torsion angle dynamics for NMR structure calculation with the new program DYANA. *J. Mol. Biol. 273*, 283–298.
22. Cornilescu, G., Delaglio, F., and Bax, A. (1999) Protein backbone angle restraints from searching a database for chemical shift and sequence homology. *J. Biomol. NMR 13*, 289–302.
23. Pearlman, D. A., Case, D. A., Caldwell, J. W., Ross, W. S., Cheatham, T. E., Debolt, S., Ferguson, D., Seibel, G., and Kollman, P. (1995) Amber, a Package of Computer-Programs for Applying Molecular Mechanics, Normal-Mode Analysis, Molecular-Dynamics and Free-Energy Calculations to Simulate the Structural and Energetic Properties of Molecules. *Comput. Phys. Commun. 91*, 1–41.
24. Mei, Y., Xie, C., Xie, W., Wu, Z., and Wu, M. (2007) Siah-1S, a novel splice variant of Siah-1 (seven in absentia homolog), counteracts Siah-1-mediated downregulation of β-catenin. *Oncogene 26*, 6319–6331.
25. Rety, S., Osterloh, D., Arie, J. P., Tabaries, S., Seeman, J., Russo-Marie, F., Gerke, V., and Lewit-Bentley, A. (2000) Structural basis of the Ca^{2+}-dependent association between S100C (S100A11) and its target, the N-terminal part of annexin I. *Structure 8*, 175–184.
26. Rustandi, R. R., Baldisseri, D. M., and Weber, D. J. (2000) Structure of the negative regulatory domain of p53 bound to S100B($\beta\beta$). *Nat. Struct. Biol. 7*, 570–574.
27. Inman, K. G., Yang, R., Rustandi, R. R., Miller, K. E., Baldisseri, D. M., and Weber, D. J. (2002) Solution NMR structure of S100B bound to the high-affinity target peptide TRTK-12. *J. Mol. Biol. 324*, 1003–1014.
28. Bhattacharya, S., Large, E., Heizmann, C. W., Hemmings, B., and Chazin, W. J. (2003) Structure of the Ca^{2+}/S100B/NDR kinase peptide complex: Insights into S100 target specificity and activation of the kinase. *Biochemistry 42*, 14416–14426.
29. Rety, S., Sopkova, J., Renouard, M., Osterloh, D., Gerke, V., Tabaries, S., Russo-Marie, F., and Lewit-Bentley, A. (1999) The crystal structure of a complex of p11 with the annexin II N-terminal peptide. *Nat. Struct. Biol. 6*, 89–95.
30. Wilder, P. T., Lin, J., Bair, C. L., Charpentier, T. H., Yang, D., Liriano, M., Varney, K. M., Lee, A., Oppenheim, A. B., Adhya, S., Carrier, F., and Weber, D. J. (2006) Recognition of the tumor suppressor protein p53 and other protein targets by the calcium-binding protein S100B. *Biochim. Biophys. Acta 1763*, 1284–1297.
31. McClintock, K. A., and Shaw, G. S. (2003) A novel S100 target conformation is revealed by the solution structure of the Ca^{2+}-S100B-TRTK-12 complex. *J. Biol. Chem. 278*, 6251–6257.
32. Benesch, J. L., Ruotolo, B. T., Simmons, D. A., and Robinson, C. V. (2007) Protein complexes in the gas phase: Technology for structural genomics and proteomics. *Chem. Rev. 107*, 3544–3567.
33. Maler, L., Sastry, M., and Chazin, W. J. (2002) A structural basis for S100 protein specificity derived from comparative analysis of apo and Ca^{2+}-calcyclin. *J. Mol. Biol. 317*, 279–290.
34. Otterbein, L. R., Kordowska, J., Witte-Hoffmann, C., Wang, C. L., and Dominguez, R. (2002) Crystal structures of S100A6 in the Ca^{2+}-free and Ca^{2+}-bound states: The calcium sensor mechanism of S100 proteins revealed at atomic resolution. *Structure 10*, 557–567.
35. Ostendorp, T., Leclerc, E., Galichet, A., Koch, M., Demling, N., Weigle, B., Heizmann, C. W., Kroneck, P. M., and Fritz, G. (2007) Structural and functional insights into RAGE activation by multimeric S100B. *EMBO J. 26*, 3868–3878.
36. Tetsu, O., and McCormick, F. (1999) β-Catenin regulates expression of cyclin D1 in colon carcinoma cells. *Nature 398*, 422–426.
37. Lin, S. Y., Xia, W. Y., Wang, J. C., Kwong, K. Y., Spohn, B., Wen, Y., Pestell, R. G., and Hung, M. C. (2000) β-Catenin, a novel prognostic marker for breast cancer: Its roles in cyclin D1 expression and cancer progression. *Proc. Natl. Acad. Sci. U.S.A. 97*, 4262–4266.
38. Schafer, B. W., and Heizmann, C. W. (1996) The S100 family of EF-hand calcium-binding proteins: Functions and pathology. *Trends Biochem. Sci. 21*, 134–140.
39. Weterman, M. A. J., Stoopen, G. M., Vanmuijen, G. N. P., Kuznicki, J., Ruiter, D. J., and Bloemers, H. P. J. (1992) Expression of Calcyclin in Human-Melanoma Cell-Lines Correlates with Metastatic Behavior in Nude-Mice. *Cancer Res. 52*, 1291–1296.
40. Hsieh, H. L., Schafer, B. W., Sasaki, N., and Heizmann, C. W. (2003) Expression analysis of S100 proteins and RAGE in human tumors using tissue microarrays. *Biochem. Biophys. Res. Commun. 307*, 375–381.

41. Sanders, M. E., Dias, E. C., Xu, B. J., Mobley, J. A., Billheimer, D., Roder, H., Grigorieva, J., Dowsett, M., Arteaga, C. L., and Caprioli, R. M. (2008) Differentiating proteomic biomarkers in breast cancer by laser capture microdissection and MALDI MS. *J. Proteome Res. 7*, 1500–1507.
42. Sun, S. R., Ning, X. X., Liu, J., Liu, L., Chen, Y., Han, S., Zhan, Y. Q., Liang, J., Wu, K. C., and Fan, D. M. (2007) Overexpressed CacyBP/SIP leads to the suppression of growth in renal cell carcinoma. *Biochem. Biophys. Res. Commun. 356*, 864–871.
43. Correia, J. D., Miranda, Y., Leonard, N., and Ulevitch, R. (2007) SGT1 is essential for Nod1 activation. *Proc. Natl. Acad. Sci. U.S.A. 104*, 6764–6769.
44. Splechowicz, M., Zylicz, A., Bleganowski, P., Kuznicki, J., and Filipek, A. (2007) Hsp70 is a new target of Sgt1: An interaction modulated by S100A6. *Biochem. Biophys. Res. Commun. 357*, 1148–1153.
45. Slomnicki, L. P., Nawrot, B., Lesniak, W. (2008) S100A6 interacts with p53 and affects its activity. *Int. J. Biochem. Cell Biol* in press, doi: 10.1016/j.biocel.2008.08.007.

BI801233Z